

# Evidence for a floating phase of the transverse ANNNI model at high frustration

Matteo Beccaria,<sup>1,\*</sup> Massimo Campostrini,<sup>2,†</sup> and Alessandra Feo<sup>3,‡</sup>

<sup>1</sup>*Dipartimento di Fisica dell'Università di Lecce and I.N.F.N.,  
Sezione di Lecce, Via Arnesano, 73100 Lecce, Italy*

<sup>2</sup>*Dipartimento di Fisica dell'Università di Pisa and I.N.F.N.,  
Sezione di Pisa, Largo Bruno Pontecorvo 3, 56127 Pisa, Italy*

<sup>3</sup>*Dipartimento di Fisica dell'Università di Parma and I.N.F.N.,  
Gruppo coll. di Parma, Viale G. P. Usberti 7/A, 43100 Parma, Italy*

(Dated: February 28, 2007)

## Abstract

We study the transverse quantum ANNNI model in the region of high frustration ( $\kappa > 0.5$ ) using the DMRG algorithm. We obtain a precise determination of the phase diagram, showing clear evidence for the existence of a floating phase, separated from the paramagnetic modulated phase by a high-order critical line ending at the multicritical point. We obtain simple and accurate formulae for the two critical lines.

PACS numbers: 67.40.-w, 05.70.Jk, 64.60.Fr, 11.15.Me

## I. THE MODEL

The ANNNI model is an axial Ising model with competing next-nearest-neighbor antiferromagnetic coupling in one direction. It is a paradigm for the study of competition between magnetic ordering, frustration and thermal disordering effects.

In the Hamiltonian limit, we consider a one-dimensional quantum spin  $S = \frac{1}{2}$  chain interacting with an external magnetic field, called the TAM model (transverse ANNNI).

The TAM Hamiltonian for  $L$  spins with open boundary conditions reads<sup>1,2</sup>

$$H = -J_1 \sum_{i=1}^{L-1} \sigma_i^z \sigma_{i+1}^z - J_2 \sum_{i=1}^{L-2} \sigma_i^z \sigma_{i+2}^z - B \sum_{i=1}^L \sigma_i^x. \quad (1)$$

We use the “traditional” notation  $\kappa = -J_2/J_1$ . The notations  $\lambda = J_1/B$  and  $\Gamma = B$  are sometimes used in the literature.

The sign of  $J_1$  is immaterial, since the Hamiltonian is invariant under the transformation

$$J_1 \rightarrow -J_1, \quad \sigma_i^y \rightarrow (-1)^i \sigma_i^y, \quad \sigma_i^z \rightarrow (-1)^i \sigma_i^z. \quad (2)$$

Likewise, the sign of  $B$  is immaterial. Without loss of generality, we set  $J_1 = 1$ . We restrict ourselves to positive  $\kappa$  and even  $L$ .

We also consider fixed boundary conditions, where we add to the extremities of the chain two fixed spins  $\sigma_0$  and  $\sigma_{L+1}$ , with the possibilities of parallel ( $\sigma_0, \sigma_{L+1} = \uparrow\uparrow$ ) or antiparallel ( $\sigma_0, \sigma_{L+1} = \uparrow\downarrow$ ) boundary conditions.

In the region of high frustration ( $\kappa > 0.5$ ), despite extensive studies<sup>3-7</sup>, the phase diagram of the transverse ANNNI model is not well known. For low  $B$ , the model is known to be in the gapless “antiphase”  $\uparrow\uparrow\downarrow\downarrow$ . It undergoes a second-order phase transition at a magnetic field  $B_1(\kappa)$ . The existence of a “floating” phase, massless and with slowly decaying spin correlation functions, up to a Kosterlitz-Thouless phase transition at a magnetic field  $B_2(\kappa)$ , is an open question. For high  $B$ , the TAM is known to be in a paramagnetic modulated phase.

## II. OBSERVABLES

We measure the two lowest energies  $E_0$  and  $E_1$ , the mass gap  $\Delta = E_1 - E_0$ , the entanglement entropy  $S_A$  (see below), and two spin-spin correlation functions: the “slow” correlation

function

$$c_s(d) = \langle \sigma_{L/2+1}^z \sigma_{L/2+1+d}^z \rangle, \quad 1 \leq d \leq L/2 \quad (3)$$

and the “fast” correlation function

$$c_f(d) = \langle \sigma_{L/2-d}^z \sigma_{L/2+1+d}^z \rangle, \quad 0 \leq d \leq L/2. \quad (4)$$

Interesting quantities related to the correlation functions are:

the overlap  $o$  of  $c_s(d)$  with the antiphase correlation function

$$c_a(d) = (-1)^{\lfloor (d-L/2)/2 \rfloor}, \quad o = \frac{2}{L} \sum_{d=1}^{L/2} c_f(d) c_a(d); \quad (5)$$

the average fast correlation function (times an oscillating sign)

$$\bar{c}_f = (-1)^{L/2} \frac{2}{L+2} \sum_{d=0}^{L/2} c_f(d); \quad (6)$$

the range of the fast correlation function

$$R = \frac{\sum_{d=0}^{L/2} d c_f^2(d)}{\sum_{d=0}^{L/2} c_f^2(d)}. \quad (7)$$

### A. Entanglement entropy

It is possible to study an order-disorder phase transition using the entanglement entropy<sup>8</sup>. We divide the system of size  $L$  into a left subsystem of size  $\ell$  and a right subsystem of size  $L - \ell$ , and define

$$S_A(\ell; L) = -\text{Tr}(\rho_A \ln \rho_A), \quad (8)$$

where  $A$  denotes the degrees of freedom of the left subsystem,  $B$  the degrees of freedom of the right subsystem, and  $\rho_A = \text{Tr}_B |\Psi_0\rangle\langle\Psi_0|$ ; note that  $S_A(\ell; L) = S_A(L-\ell; L)$ . For a critical system we expect (neglecting lattice artifacts)

$$S_A(\ell; L) \sim (c/6) \log(L \sin(\pi\ell/L)), \quad (9)$$

where  $c$  is the conformal anomaly number (central charge) of the corresponding conformal field theory, and  $\sim$  means “up to a (non-universal) additive constant”; for the case of interest for the infinite-volume DMRG,  $\ell = \frac{1}{2}L$ , and  $\sin(\pi\ell/L)$  only shifts the additive constant. For a noncritical system, we expect

$$S_A(\frac{1}{2}L; L) \sim (c/6)[\log L + s(L/\xi)], \quad (10)$$

where  $s(x)$  is a *universal* finite-size scaling function satisfying the constraints  $s(0) = 0$  and  $s(x) \sim -\log x$  for large  $x$ .

## B. Domain-wall energy

So far, we only considered open boundary conditions. Following Ref. 9, we define the domain-wall energy (note that our definition of  $L$  differs by 2 from the definition of Ref. 9)

$$E_{\text{DW}}(\kappa, B, L) = (-1)^{L/2+1} \left[ E_0^{\uparrow\uparrow}(\kappa, B, L) - E_0^{\uparrow\downarrow}(\kappa, B, L) \right], \quad (11)$$

where  $E_0^{\uparrow\uparrow}$  and  $E_0^{\uparrow\downarrow}$  are the ground state energies with parallel and antiparallel boundary conditions respectively.

## III. THE ALGORITHM

We implement the density matrix renormalization group (DMRG) algorithm described in Ref. 10. We sample the  $n_s$  lowest energy levels with equal weights, i.e., we use the reduced density matrix

$$\hat{\rho}_S = \frac{1}{n_s} \text{Tr}_E \sum_{i=0}^{n_s-1} |\psi_i\rangle \langle \psi_i| \quad (12)$$

(see Eq. (26) of Ref. 10). Usually, since we are interested in the mass gap  $\Delta$ , we set  $n_s = 2$ . We identify system and environment (for antiparallel boundary conditions, up to a spin flip  $\sigma_i^y \rightarrow -\sigma_i^y$ ,  $\sigma_i^z \rightarrow -\sigma_i^z$ ). The typical dimension of the truncated system and environment is  $M = 80$ .

The crucial part of the numerical computation is finding the lowest eigenvalues and eigenvectors of the superblock Hamiltonian; we employ the Implicitly Restarted Arnoldi Algorithm implemented in Arpack<sup>11</sup>, in the routine `dsaupd` used in mode 1. We use (typically) 100 Lanczos vectors and require convergence to machine precision, obtaining residual norms  $|Hx - \lambda x|/|\lambda| \sim 10^{-14}$ .

We observe a truncated weight (the sum of the eigenvalues of the density matrix whose eigenvectors are dropped in the truncation)  $\varepsilon \sim 10^{-8}$  for “normal” configurations, and  $\varepsilon \sim 10^{-7}$  for peaks of  $\Delta$  (see below).

We managed to diagonalize the system exactly up to  $L = 18$ ; both the finite- and the infinite-volume DMRG algorithm reproduce the results of exact diagonalization. For moder-

ate  $L$ , finite- and the infinite-volume DMRG give consistent results. For higher  $L$ , discrepancies between finite- and infinite-volume DMRG and  $M$ -dependence of  $\Delta$  becomes noticeable; they are strongly observable-dependent, and they will be discussed below, where results on observables are presented.

In the finite-volume DMRG algorithm, we keep in memory the system/environment for all smaller lattice sizes; therefore, it is possible to estimate the observables at all  $L$ s smaller than  $L_n$  (the “nominal”  $L$  of the run), with a moderate numerical effort (just one extra diagonalization and measurement, without rotation and truncation, for each lattice size). These estimates almost coincide with the results obtained running independently at each  $L$ .

The finite-volume DMRG algorithm at large  $L$  requires a very large amount of memory; however, since the observables at each lattice size are accessed only twice per cycle, they can be conveniently kept on disk, requiring only a very large amount of disk space; for  $L = 600$  and  $M = 80$ , e.g., ca. 6 Gbytes are required.

#### IV. PHASES AT $\kappa = 0.75$

We will first focus our attention on the model at  $\kappa = 0.75$ , and later on extend the study to other values of  $\kappa$ .

Running the infinite-volume DMRG algorithm at  $\kappa = 0.75$  and  $B \leq 0.257$ , with open boundary conditions, we observe that the mass gap  $\Delta$  vanishes exponentially in  $L$ , apart from numerical errors due to the fact that  $\Delta$  is computed as  $E_1 - E_0$ : see, e.g., Fig. 1.

The slow correlation function  $c_s(d)$  almost coincides with  $c_a(d)$ ; the overlap  $o$  approaches a value very close to 1 with corrections proportional to  $1/L$ . The fast correlation function  $c_s(d)$  is constant and close to  $\pm 1$ , apart from  $d = 0$  and  $ds$  close to  $L/2$ ; the range  $R$  is almost exactly  $L/4$  (the value for a constant  $c_f(d)$ ) and the average  $\bar{c}_f$  approaches a value very close to  $-1$  with corrections proportional to  $1/L$ .

There is a very sharp phase transition at  $0.257 < B_1 < 0.258$ . We will postpone its detailed study, since it is best done using  $E_{\text{DW}}$ .

Running at  $\kappa = 0.75$  and  $B \geq 0.258$ , the mass gap  $\Delta$  as a function of  $L$  at fixed  $B$  shows sharp peaks with a frequency increasing with  $B$ : see Fig. 2. Each peak match exactly a change of sign of  $\bar{c}_f$ . At each  $B$ , for  $L$  smaller than the first peak we observe signals very similar to the case  $B \leq 0.257$ ; for higher  $L$ , we observe that the minima of  $\Delta$  seem to go

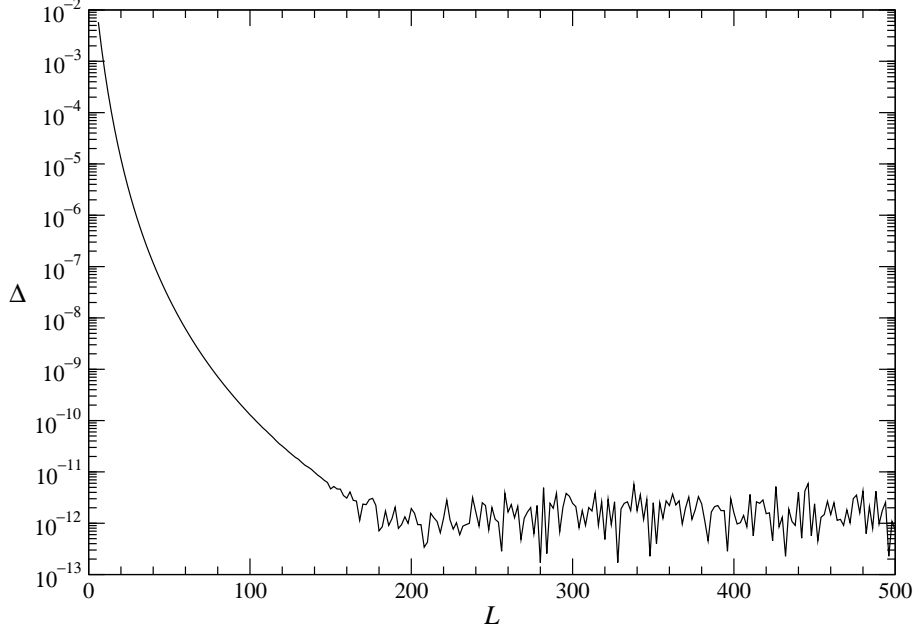


FIG. 1: Mass gap vs.  $L$  for  $\kappa = 0.75$  and  $B = 0.257$ . To appreciate the effect of numerical errors, note that  $E_0(B=0.257) \cong -0.8L$ .

to zero for  $B \leq 0.4$  and to a nonzero limit for  $B \geq 0.5$ ; however, the determination of  $\Delta$  from the infinite-volume DMRG is not accurate for  $L \gtrsim 200$ ; finite-volume DMRG data with  $M = 80$  become unreliable for  $L > 300$ ; we show in Fig. 3 the case  $B = 0.3$ .

We performed a finite-size analysis of  $\Delta$ , looking for the intersections  $B_i(L_1, L_2)$  of the curves  $L\Delta_L(B, \kappa)$  vs.  $B$  at two fixed values  $L_1$  and  $L_2$ . This case is much more harder than the case  $\kappa < 0.5$  considered in Ref. 2, due to the peak structure; we defined  $\Delta_L(B, \kappa)$  from the data at the minima in  $L$ , performing an interpolation (at fixed  $B$  and  $\kappa$ ) to obtain  $\Delta_L(B, \kappa)$  at the desired values of  $L$ ;  $\Delta_L(B, \kappa)$  is then interpolated in  $B$  (at fixed  $L$  and  $\kappa$ ) as needed; analyzing finite-volume DMRG data<sup>14</sup> with  $L_n \geq 292$  at  $B = 0.4, 0.41, 0.42, 0.43, 0.44, 0.45, 0.46$ , we obtain  $B_2 = 0.424(3)$ : see Fig. 4.

For  $0.258 \leq B \lesssim 0.45$ , the slow correlation function  $c_s(d)$  at fixed  $L$  shows the expected behavior of a floating phase,

$$c_s(d) \cong ad^{-\eta} \cos(qd + \phi), \quad (13)$$

with  $\eta$  increasing from 0 for  $B = 0.258$  to  $\eta \cong \frac{1}{3}$  for  $B = 0.45$ . For  $B \geq 0.5$ ,  $c_s(d)$  at fixed  $L$  shows the expected behavior of a paramagnetic modulated phase,

$$c_s(d) \cong a \exp(-\lambda d) \cos(qd + \phi). \quad (14)$$

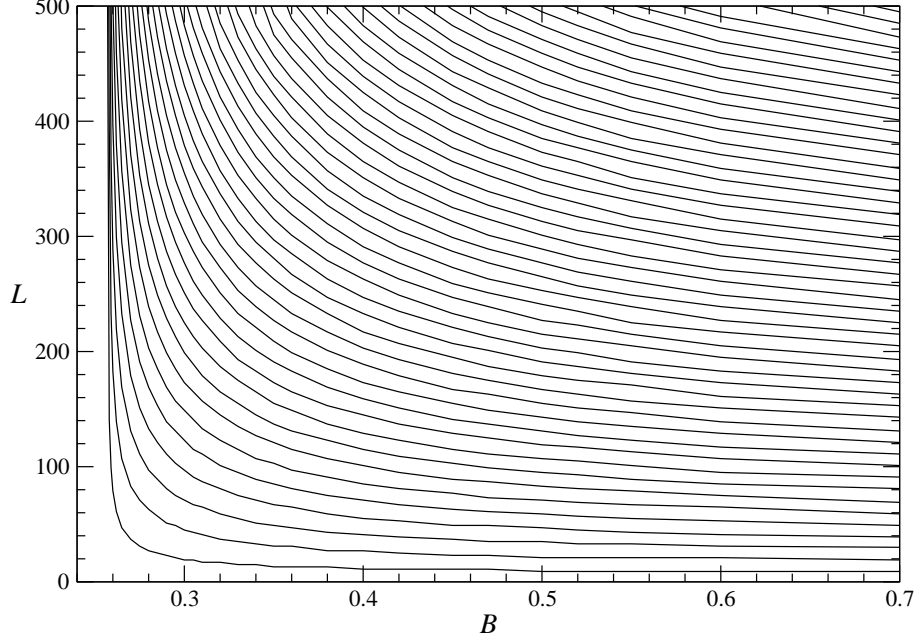


FIG. 2: Mass gap peaks in the  $L$ - $B$  plane for  $\kappa = 0.75$ .

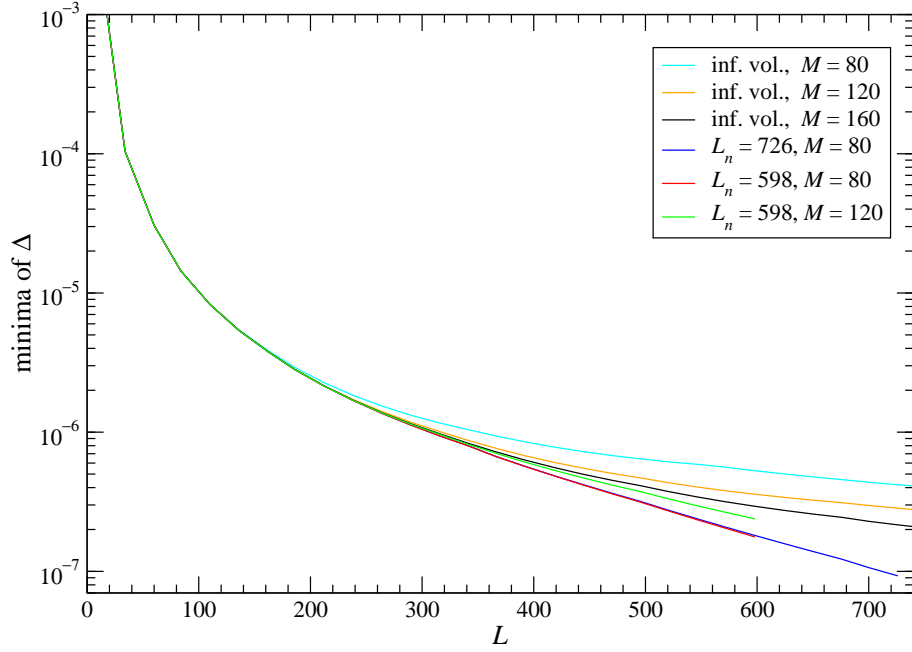


FIG. 3: Minima of mass gap  $\Delta$  vs.  $B$  for  $\kappa = 0.75$  and  $B = 0.3$ .

We tried to extract  $\eta$  by fitting  $c_s^2(d)$ , smoothed by taking a running average over  $\lfloor 2\pi/q + \frac{1}{2} \rfloor$  points, to the form  $ad^{-2\eta}$ . In Fig. 5 we show the typical case  $B = 0.425$ ;  $c_s^2(d)$  for different values of  $L$  converge not to a single curve but to two separate curves, with different values of  $\eta$ , preventing a precise determination of  $\eta$ .

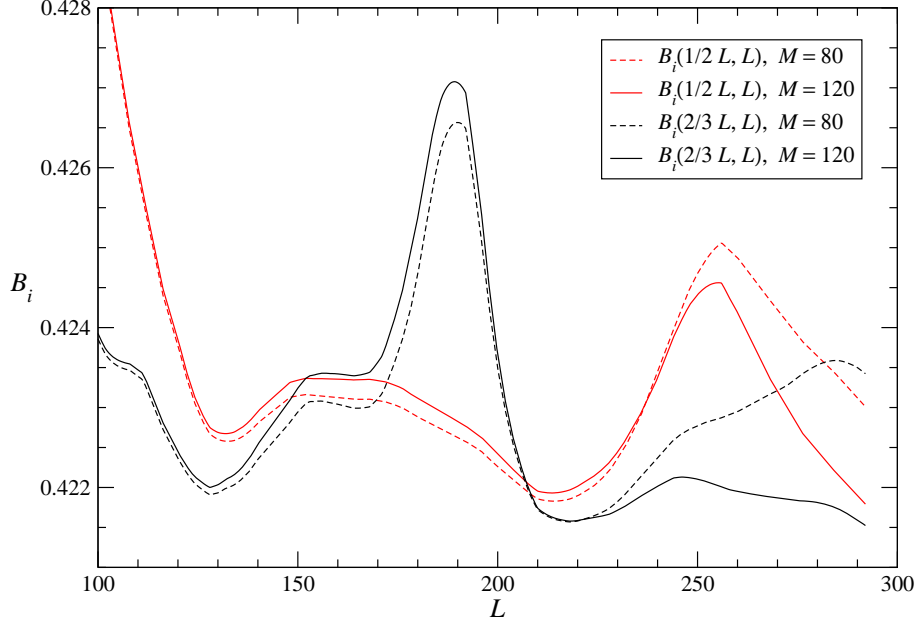


FIG. 4: The intersection  $B_i$  vs.  $L$ , for  $\kappa = 0.75$ .

The range of the fast correlation function  $R$  should distinguish clearly the floating phase, where  $R \rightarrow \infty$  as  $L \rightarrow \infty$  (since  $\eta < \frac{1}{2}$ ), from the paramagnetic phase, where  $R$  has a finite limit as  $L \rightarrow \infty$ . A first problem is the presence of oscillations, with dips corresponding to the peaks of  $\Delta$  (see Fig. 6); it is solved by selecting the values of  $R$  at the  $L$ s corresponding to the peaks of  $\Delta$ . After this operation,  $R$  vs.  $L$  at fixed  $B$  and  $M$  is well fitted to the form

$$R(L) = \frac{s_R L^2 + pL}{L + q}; \quad (15)$$

if we plot the asymptotic slope  $s_R$  vs.  $B$  we should be able to see a drop towards 0 in correspondence with the phase transition. However, in the critical region,  $R$  (and  $s_R$ ) strongly depend on  $M$ : see Fig. 6; we can only conclude that  $B_2 \simeq 0.45$ .

The analysis of the range of the slow correlation function gives similar, but even less precise, results.

### A. Entanglement entropy

The simple Ansatz for the finite-size scaling function entering Eq. (10),

$$s(x) = -\ln(x + e^{-\alpha x}) \quad (16)$$



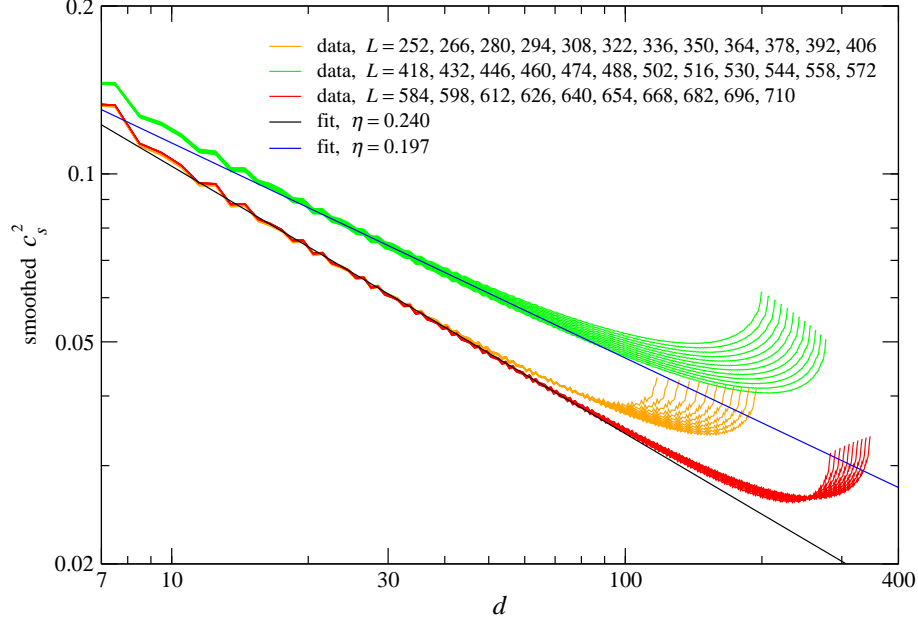


FIG. 5: The smoothed squared slow correlation function  $c_s^2(d)$  for  $\kappa = 0.75$  and  $B = 0.425$ , from the finite-volume DMRG at  $L_n = 710$  and  $M = 120$ , for values of  $L$  corresponding to minima of  $\Delta$ .

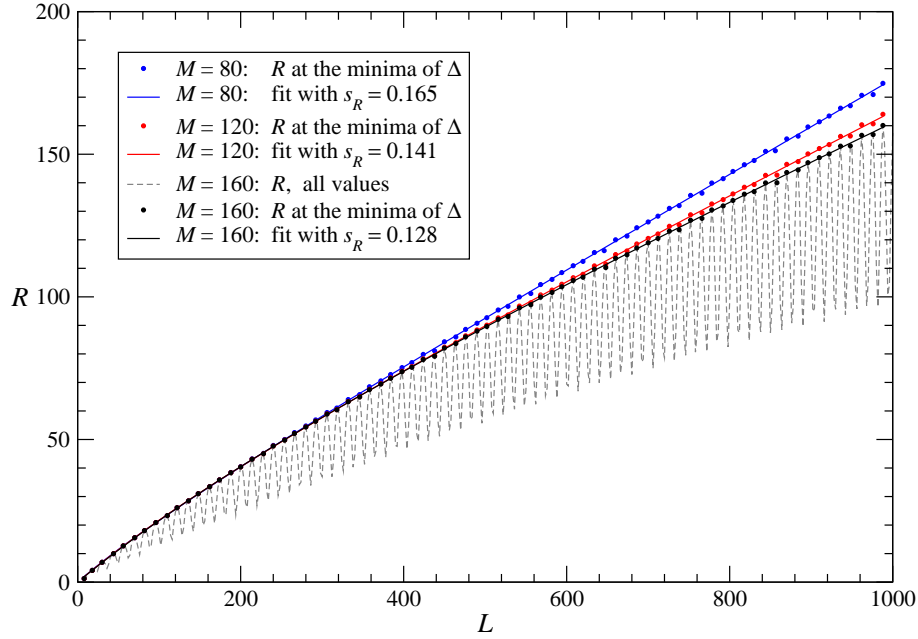


FIG. 6:  $R$ , at the  $L$ s corresponding to minima of  $\Delta$ , with fits to Eq. (15), for  $\kappa = 0.75$ ,  $B = 0.45$  and different  $M$ s. For  $M = 160$ , all the values of  $R$  are also plotted.

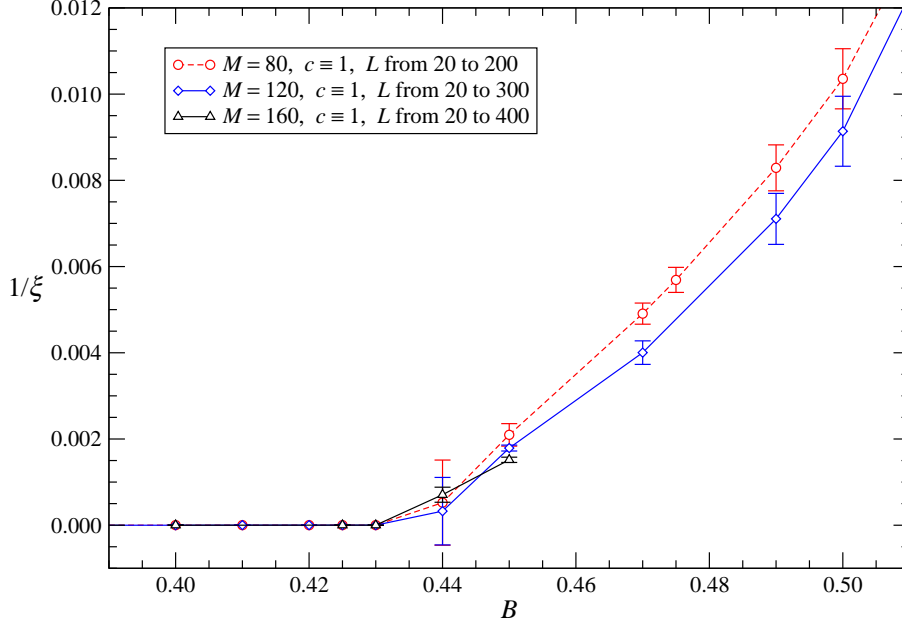


FIG. 7: The reciprocal correlation length  $1/\xi$  (determined from  $S_A$ ) vs.  $B$ , for  $\kappa = 0.75$ .

with  $\alpha \equiv 1$ , is found to fit the entanglement entropy data very well (excluding just the very smallest lattices with  $L \lesssim 10$ ) in all cases for the floating and paramagnetic phases.

We estimate that the infinite-volume DMRG determination of  $S_A$  is reliable up to  $L \simeq 200$  for  $M = 80$  and up to  $L \simeq 300$  for  $M = 120$ . In the antiphase,  $S_A$  is essentially constant, indicating a very small correlation length. In the floating and paramagnetic phases,  $c$  is always compatible with 1; the best determination of  $\xi$  is obtained by fitting  $S_A$  with  $c \equiv 1$  fixed. We obtain  $B_2 \simeq 0.44$ : see Fig. 7.

As we can see from Fig. 8, finite-volume DMRG essentially reproduces the results of infinite-volume DMRG at the same  $M$ .

## B. Domain-wall energy

So far, we only considered open boundary conditions. We now switch to fixed boundary conditions, in order to compute the domain-wall energy  $E_{\text{DW}}$ ; with fixed boundary conditions, there are no problems with quasi-degenerate energy levels (typically,  $\Delta > 0.01$ ) or peaks in  $\Delta$  associated with level crossings, and truncated weights are  $\varepsilon \sim 10^{-9}$  or smaller for  $M = 80$ . Even if we are not interested in the mass gap, we run with  $n_s = 2$ , which gives results more stable than  $n_s = 1$ .

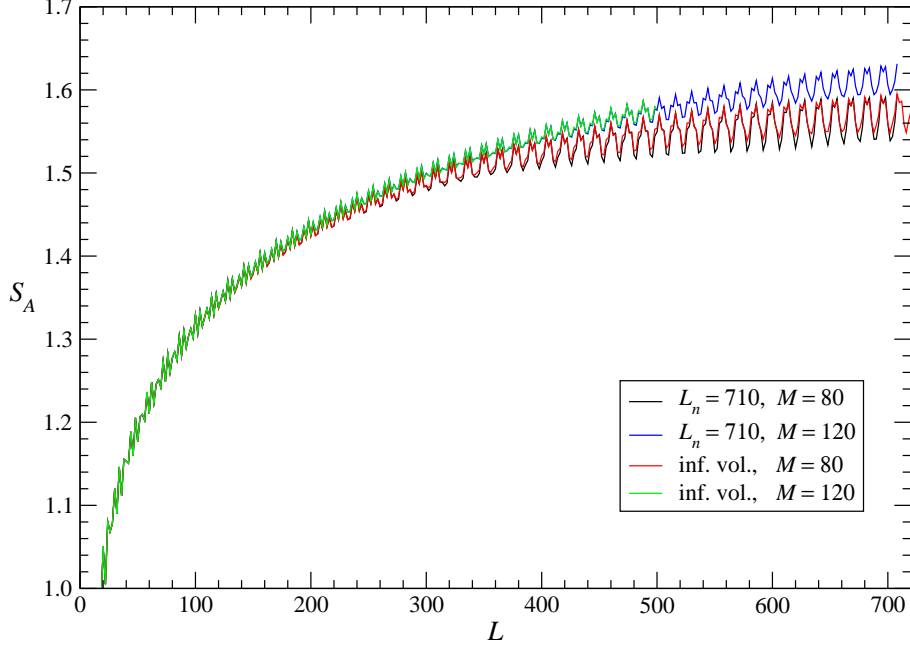


FIG. 8: The entanglement entropy  $S_A(\frac{1}{2}L; L)$  vs. the size of the system  $L$ , for  $\kappa = 0.75$ ,  $B = 0.425$ ,  $L_n = 710$ , and infinite-volume DMRG.

We may fit  $E_{\text{DW}}$  to the form

$$E_{\text{DW}} = a \exp(-dL)L^{-\nu} + E_{\infty} \quad (17)$$

in the antiphase and

$$E_{\text{DW}} = \frac{a \exp(-dL)}{L} \left[ |\cos(kL + \phi)| - |\sin(kL + \phi)| \right] \quad (18)$$

in the floating phase (with  $d = 0$ ) and in the paramagnetic phase<sup>9</sup>. The fits, excluding (typically) lattices with  $L < 16$ , are of very good quality and stable.

Eq. (17), fits perfectly  $E_{\text{DW}}$  for  $B \leq 0.257$ , giving  $E_{\infty} \rightarrow 0$ , constant  $\nu \simeq 1.6$  and  $d \simeq 0.008$  for  $B \nearrow B_1$ . Eq. (18), with  $d = 0$ , fits perfectly  $E_{\text{DW}}$  for  $B > 0.257$  and gives  $k \rightarrow 0$  for  $B \searrow B_1$ . The best estimators of  $B_1$  are  $E_{\infty}$  in the antiphase and  $k^2$  in the floating phase, both vanishing linearly at  $B_1$ , see Figs. 9 and 10; the final estimate of the critical field is  $B_1 = 0.2574(2)$ .

So far, we obtained results very similar to those of Ref. 9. We turn now to the problem of identifying the floating phase, i.e., a region with  $d = 0$ . The data generated with the infinite-volume DMRG at  $0.3 < B < 0.4$  seem to indicate  $d < 0$ ; this appears to be an

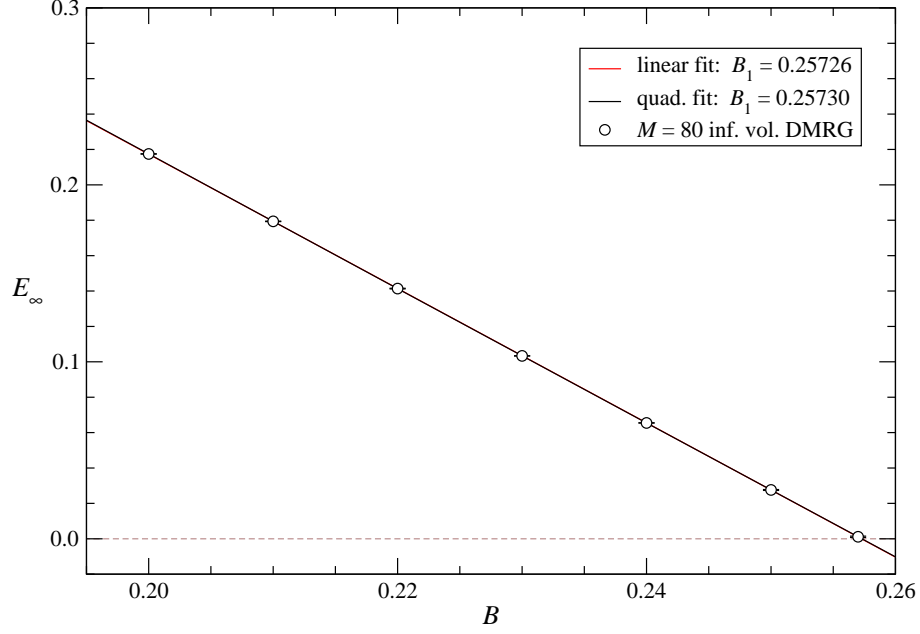


FIG. 9: The infinite-volume domain-wall energy  $E_\infty$  vs.  $B$ , for  $\kappa = 0.75$ .

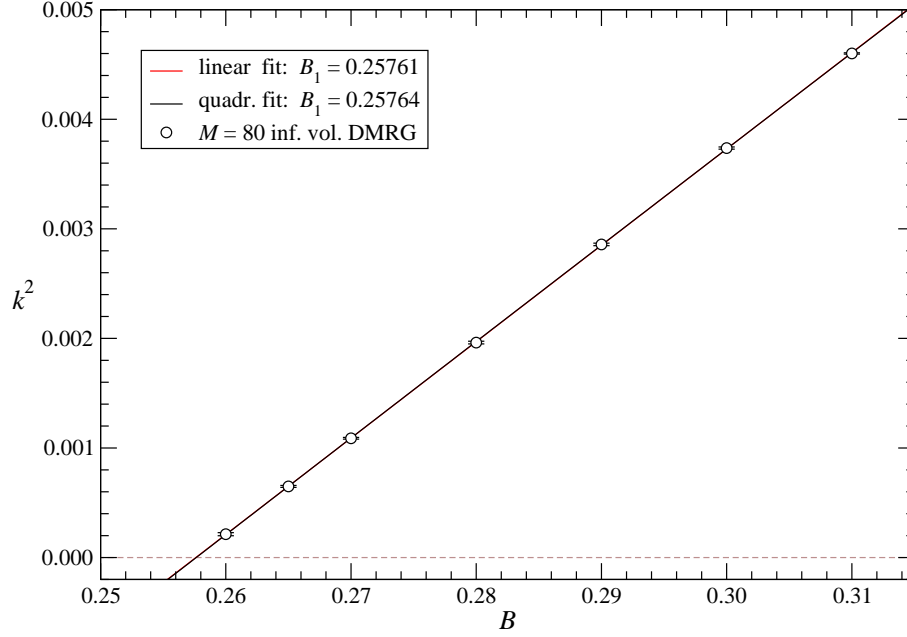


FIG. 10: The squared modulation parameter  $k^2$  vs.  $B$ , for  $\kappa = 0.75$ .

artifact of the infinite-volume DMRG, as we can see from the comparison of  $E_{\text{DW}}$  evaluated with the finite- and infinite-volume DMRG at  $B = 0.3$ , shown in Fig. 11.

We must therefore resort to the resource-consuming finite-volume DMRG. We show the results in Fig. 12. The value of  $d$  obtained from the finite-volume DMRG is consistent with

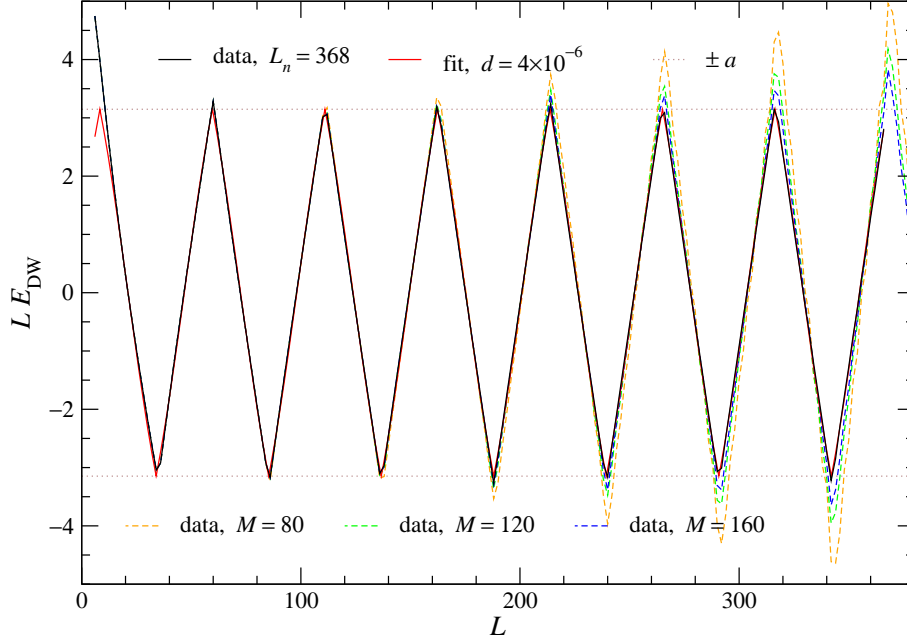


FIG. 11: Determinations of the domain-wall energy  $E_{\text{DW}}$ , multiplied by  $L$ , vs.  $L$ , for  $\kappa = 0.75$  and  $B = 0.3$ : finite-volume DMRG at  $M = 80, 120, 160$ ; infinite-volume DMRG at  $L_n = 368, M = 80$ ; fit to Eq. (18) of the  $L_n = 368$  data.

zero up to  $B = 0.425$ , where we estimate  $\xi \equiv 1/d > 10^4$ . The smoothness of  $d$  vs.  $B$  suggest a higher-order, possibly Kosterlitz-Thouless, phase transition. Note that  $d$  is quite compatible with  $1/\xi$  of Fig. 7 (apart from a normalization stemming from the different definition of correlation length), and so is the resulting  $B_1 = 0.435(10)$ .

Finally, we can conclude that all the determinations of  $B_2$  are consistent with each other.

## V. PHASE DIAGRAM

The study of the phase transitions at other values of  $\kappa$ s is very similar to the one at  $\kappa = 0.75$  presented in Sect. IV and we can avoid repeating the details. We selected for our analysis the values  $\kappa = 0.5, 0.52, 0.55, 0.6, 0.75, 1.0, 1.25, 1.5, 2.0, 5.0$ .

At  $\kappa = 0.5$ , the DMRG algorithm becomes inefficient at low  $B$ , and we are unable to run at  $B < 0.01$ . We see no sign of a floating phase: the curves  $L\Delta_L(B, \kappa)$  vs.  $B$  almost coincide for  $0.01 < B < 0.05$ , and the intersections are very unstable. Determining  $\xi$  by fitting  $S_A$  with  $c \equiv 1$  fixed, we see no sign of  $\xi = \infty$  for  $B \geq 0.02$ , see Fig. 13. The analysis of  $E_{\text{DW}}$  does not give precise results for  $B_2$ . The behavior of the modulation parameter  $k$

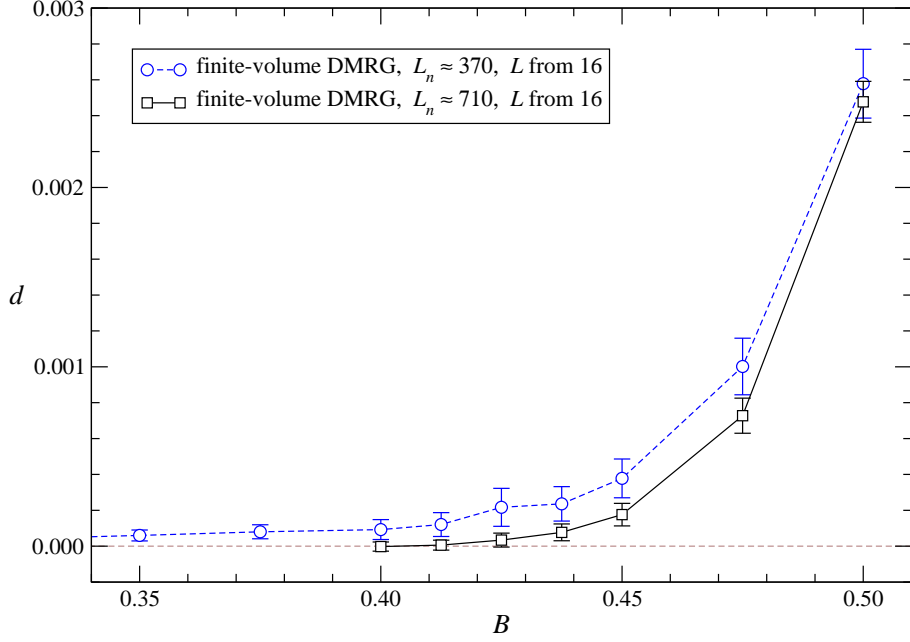


FIG. 12: The decay parameter  $d$  of the domain-wall energy  $E_{\text{DW}}$ , computed with the finite-volume DMRG, vs.  $B$ , for  $\kappa = 0.75$ .

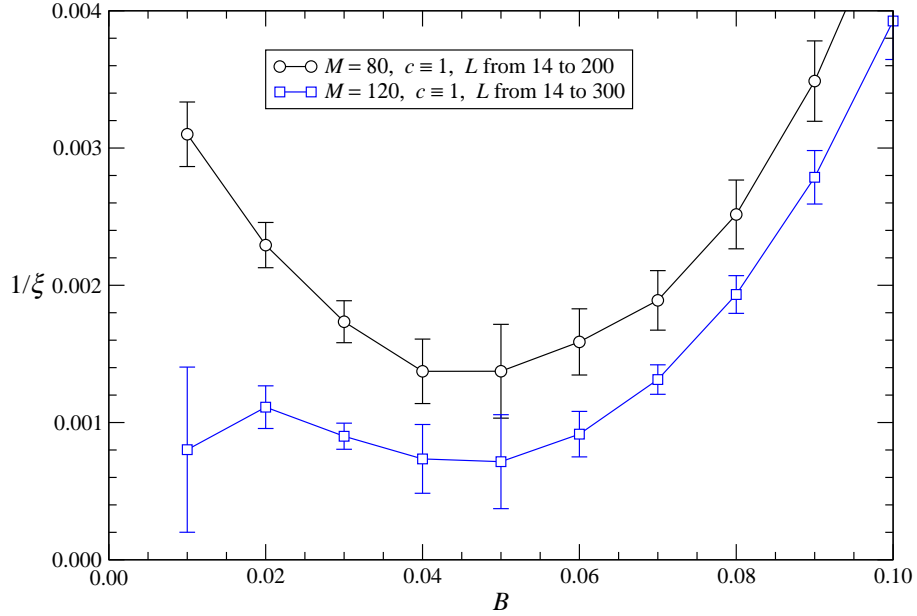


FIG. 13: The reciprocal correlation length  $1/\xi$  (determined from  $S_A$ ) vs.  $B$ , for  $\kappa = 0.5$ .

(see Fig. 14), which goes to a nonzero value as  $B \rightarrow 0$ , hints at the very peculiar nature of the multicritical point at  $\kappa = 0.5$ ,  $B = 0$ <sup>1,12</sup>.

For  $\kappa = 0.52$  and  $0.55$ , the quality of the determinations of  $B_1$  and of the determination

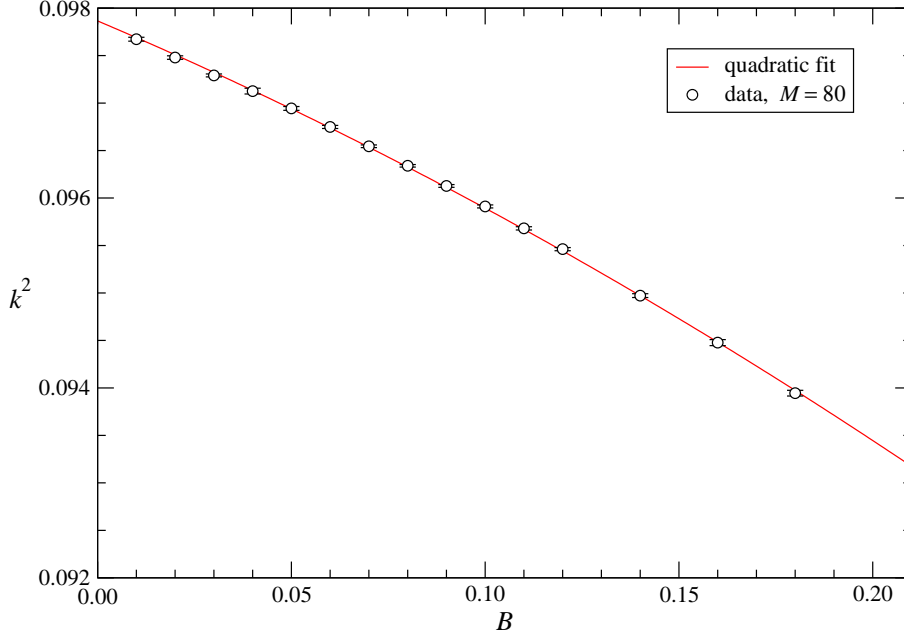


FIG. 14: The squared modulation parameter  $k^2$  vs.  $B$ , for  $\kappa = 0.5$ .

of  $B_2$  from  $S_A$  is similar to those at  $\kappa = 0.75$ ; on the other hand, the analysis of  $\Delta_L$  and  $E_{\text{DW}}$  do not give precise results for  $B_2$ .

For  $0.6 \leq \kappa \leq 1.5$ , there are no relevant differences from the case  $\kappa = 0.75$  described in Sect. IV; we only present the determinations of  $B_1$  and  $B_2$  in Table I. For  $\kappa = 2$ , the only difference is that  $E_{\text{DW}}$  is not fitted well by Eq. (18) in the floating and paramagnetic phases, and therefore the determination of  $B_2$  from  $E_{\text{DW}}$  is unreliable.

In the case  $\kappa = 5$ , the determination of  $B_1$  and  $B_2$  is rather imprecise:  $E_{\text{DW}}$  is not fitted well by Eq. (17) in the antiphase, and it is fitted poorly by Eq. (18) in the floating and paramagnetic phases; it is very hard to get precise results from  $\Delta_L$ , since the modulation parameter is very small ( $k \lesssim 0.01$  in the floating phase). It is still possible to estimate  $B_1$  from  $o$  and  $B_2$  from  $S_A$ .

For all the values of  $\kappa$  considered, the different determinations of  $B_1$  and  $B_2$  are in substantial agreement with each other: this is a strong argument supporting the reliability of our results. It should be noticed, however, that the determination of  $B_2$  from  $\Delta_L$  is systematically lower than the determination from  $S_A$ , possibly indicating that the error on the determination from  $\Delta_L$  reported in Table I is underestimated.

We can beautifully summarize all the above results by noticing that all the determinations

$\kappa$	$B_1$ ( $E_{\text{DW}}$ )	$B_1$ ( $o$ )	$B_2$ ( $\Delta_L$ )	$B_2$ ( $S_A$ )	$B_2$ ( $E_{\text{DW}}$ )
0.5	0	0	$< 0.05$	$< 0.02$	$< 0.08$
0.52	0.0201(1)	0.021(1)	0.095(15)	0.115(5)	0.12(3)
0.55	0.0501(2)	0.052(2)	0.160(15)	0.175(5)	0.18(2)
0.6	0.1015(2)	0.103(2)	0.235(6)	0.25(1)	0.25(1)
0.75	0.2574(2)	0.2575(5)	0.424(3)	0.44(1)	0.425(10)
1.0	0.5213(2)	0.522(2)	0.700(5)	0.72(1)	0.71(1)
1.25	0.7867(2)	0.785(2)	0.972(4)	1.00(1)	0.98(1)
1.5	1.0514(2)	1.045(5)	1.235(3)	1.26(1)	1.26(1)
2.0	1.5775(2)	1.576(2)	1.756(6)	1.79(1)	1.79(3)
5.0	—	4.667(3)	—	4.88(1)	—

TABLE I: Determinations of the transition fields  $B_1$  and  $B_2$  by different techniques.

of  $B_1$  and  $B_2$  are consistent with

$$B_1(\kappa) \cong 1.05(\kappa - \tfrac{1}{2}), \quad B_2(\kappa) \cong 1.05\sqrt{(\kappa - \tfrac{1}{2})(\kappa - 0.1)}. \quad (19)$$

Finally, we draw the phase diagram in the  $\kappa$ - $B$  plane in Fig. 15. The region  $\kappa < 0.5$  was studied in Ref. 2; the critical line separating the paramagnetic modulated and paramagnetic unmodulated phases is known analytically<sup>13</sup>. The data in the region  $\kappa > 0.5$  are taken from the present work; note that earlier results<sup>3-6</sup> provided only a qualitative picture of the phase diagram in this region.

A very interesting question is whether the floating phase extends up to  $\kappa = \infty$  or it terminates at finite  $\kappa$ ; we found that the floating phase extends at least up to  $\kappa = 5$ .

## VI. SUMMARY AND CONCLUSIONS

We applied the DMRG algorithm to the study of the quantum transverse ANNNI model in the region of high frustration ( $\kappa > 0.5$ ).

We obtained clear evidence for the existence of a floating phase for  $\kappa > 0.5$ , extending at least up to  $\kappa = 5$ . The floating phase is separated from the paramagnetic modulated phase by a high-order (possibly Kosterlitz-Thouless) critical line, ending at the multicritical point



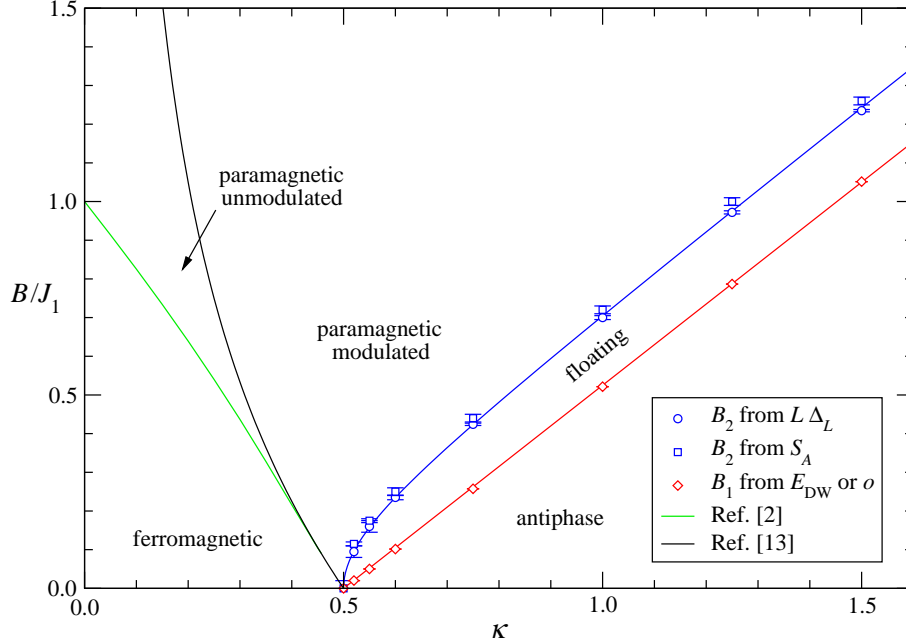


FIG. 15: Phase diagram in the  $\kappa$ - $B$  plane; the solid lines for  $\kappa \geq 0.5$  correspond to Eq. (19).

( $\kappa = 0.5$ ,  $B = 0$ ); the corresponding central charge is  $c = 1$ . In Ref. 7, the floating phase was shown to have a finite extent at  $\kappa = 0.5$ ; our study cannot exclude a floating phase of very small extent, i.e.,  $0 < B_2(\kappa=0.5) \lesssim 0.02$ .

We obtained precise estimates for the critical points, verifying that different methods give consistent results. Simple and accurate formulae for the two critical lines are reported in Eq. (19).

Very helpful discussions with Walter Selke and Pasquale Calabrese are gratefully acknowledged.

---

\* Electronic address: [matteo.beccaria@le.infn.it](mailto:matteo.beccaria@le.infn.it)

† Electronic address: [massimo.camposrini@df.unipi.it](mailto:massimo.camposrini@df.unipi.it)

‡ Electronic address: [feo@fis.unipr.it](mailto:feo@fis.unipr.it)

<sup>1</sup> W. Selke, Phys. Rep. **170**, 213 (1998).

<sup>2</sup> M. Beccaria, M. Campostrini, and A. Feo, Phys. Rev. **B 73**, 052402 (2006).

<sup>3</sup> Ph. Duxbury and M. Barber, J. Phys. **A 14**, L251 (1981).

<sup>4</sup> C. M. Arizmendi, A. H. Rizzo, L. N. Epele, and C. A. Garcia Canal, Z. Phys. **B 83**, 273 (1991).

- <sup>5</sup> P. Sen, S. Chakraborty, S. Dasgupta, and B. K. Chakrabarti, Z. Phys. **B 88**, 333 (1992).
- <sup>6</sup> P. R. Colares Guimarães, J. A. Plascak, F. C. Sà Barreto, and J. Florencio, Phys. Rev. **B66**, 064413 (2002).
- <sup>7</sup> A. K. Chandra and S. Dasgupta, Phys. Rev. **E 75**, 021105 (2007).
- <sup>8</sup> P. Calabrese and J. L. Cardy, J. Stat. Mech. **0406**, P002 (2004).
- <sup>9</sup> R. Derian, A. Gendiar, and T. Nishino, J. Phys. Soc. Jpn. **75**, 114001 (2006) (arXiv:cond-mat/0605411).
- <sup>10</sup> U. Schollwöck, Rev. Mod. Phys. **77**, 259 (2005);  
see also <http://quattro.phys.sci.kobe-u.ac.jp/dmrg.html>
- <sup>11</sup> <http://www.caam.rice.edu/software/ARPACK/>
- <sup>12</sup> P. Sen and P. K. Das, “Dynamical frustration in ANNNI model and annealing”, in “Quantum Annealing and Related Optimization Methods”, A. Das and B. K. Chakrabarti, eds., Lecture Notes in Physics 679, Springer, New York, 2005 (arXiv:cond-mat/0505027).
- <sup>13</sup> I. Peschel and V. J. Emery, Z. Phys. **B43**, 241 (1981).
- <sup>14</sup> We always run the finite-volume DMRG algorithm for  $L_n$  corresponding to a minimum of  $\Delta$ .